THE JOURNAL OF BIOLOGICAL CHEMISTRY
Vol. 278, No. 37, Issue of September 12, pp. 35292–35298, 2003
Printed in U.S.A.

Packing Interactions between Transmembrane Helices Alter Ion Selectivity of the Yeast Golgi Ca^{2+}/Mn^{2+}-ATPase PMR1*

Received for publication, June 11, 2003
Published, JBC Papers in Press, June 24, 2003, DOI 10.1074/jbc.M306166200

Debjani Mandal‡§, Samuel J. Rulli‡¶, and Rajini Rao‖

From the Department of Physiology, The Johns Hopkins University School of Medicine, Baltimore, Maryland 21205

PMR1 is the yeast secretory pathway pump responsible for high affinity transport of Mn^{2+} and Ca^{2+} into the Golgi, where these ions are sequestered and effectively removed from the cytoplasm. Phenotypic growth assays allow for convenient screening of side chains important for Ca^{2+} and Mn^{2+} transport. Earlier we demonstrated that mutant Q783A at the cytoplasmic interface of M6 could transport Ca^{2+}, but not Mn^{2+}. Scanning mutagenesis of side chains proximal to residue Gln-783 in membrane helices M2, M4, M5, and M6 revealed additional residues near the cytoplasmic interface, notably Leu-341 (M5), Phe-738 (M5), and Leu-785 (M6) that are sensitive to substitution. Importantly, we obtained evidence for a packing interaction between Val-335 in M4 and Gln-783 in M6 that is critical for Mn^{2+} transport. Thus, mutant V335G mimics the Mn^{2+} transport defect of Q783A and mutant V335I can effectively suppress the Mn^{2+}-defective phenotype of Q783A. These changes in ion selectivity were confirmed by cation-dependent ATP hydrolysis using purified enzyme. Other substitutions at these sites are tolerated individually, but not in combination. Exchange of side chains at 335 and 783 also results in ion selectivity defects, suggesting that the packing interaction may be conformation-sensitive. Homology models of M4, M5, and M6 of PMR1 have been generated, based on the structures of the sarcoplasmic reticulum Ca^{2+}-ATPase. The models are supported by data from mutagenesis and reveal that Gln-783 and Val-335 show conformation-sensitive packing at the cytoplasmic interface. We suggest that this region may constitute a gate for access of Mn^{2+} ions.

The Secretory Pathway Ca^{2+}-ATPases (SPCAs)[1] are an emerging family of Mn^{2+}- and Ca^{2+}-transporting P-type ATPases localized to the Golgi apparatus (1, 2). Members of this family have been identified in the genomes of diverse organisms, including *Saccharomyces cerevisiae* and other yeasts (PMR1), *Caenorhabditis elegans* (PMR1), *Drosophila melanogaster* (Q9VNR2), and *Homo sapiens* (ATP2C1). *S. cerevisiae* PMR1 has distinct inhibitor and transport characteristics, which clearly separate it from the well-studied sarcoendoplasmic reticulum (SERCA) and plasma membrane (PMCA) Ca^{2+}-ATPases (3, 4). Perhaps the most interesting transport characteristic of SPCA pumps is their unique ability to transport Mn^{2+} ions with high affinity (1, 2). Haploinsufficiency of the human *ATP2C1* gene for SPCA1 results in Hailey Hailey disease, characterized by acantholysis of the epidermis (5, 6).

Members of the P-ATPase superfamily share common structural and mechanistic properties yet have strikingly different ion specificities that underlie their individual physiological roles. In the reaction cycle of the P-ATPases, the E_1 conformation of the pump binds ATP and the cation(s) to be transported with high affinity, followed by transfer of the γ-phosphoryl group of ATP to an invariant aspartate to form an aspartylphosphate reaction intermediate. A major change in enzyme conformation to the E_2 form ensues, with a large reduction in ion binding affinity and reorientation of the binding pocket resulting in vectorial ion transport (7). The x-ray crystal structure of SERCA in the E_1 conformation, at 2.6-Å resolution, provides a structural definition for two high affinity Ca^{2+} binding sites enclosed by the transmembrane domains M4, M5, M6, and M8 (*8*). More recently, a second structure of the enzyme locked in the E_2 conformation, was resolved by x-ray crystallography to 3.1 Å (9). These structures revealed large domain movements within the cytoplasmic regions as well as twisting and elongation of transmembrane helices involved in cation interactions presumably during transition from the E_1 to E_2 conformations.

The repertoire of cations transported by the P-ATPases includes, but is not limited to, H^+, K^+, Na^+, Ca^{2+}, Cu^{2+}, Zn^{2+}, and Mg^{2+}. To understand the molecular basis for ion specificity, we have used phenotypic screening in yeast to identify mutations that alter selectivity for Ca^{2+} and Mn^{2+} in PMR1. Growth of the Δ*pmr1* null strain is hypersensitive to divalent cation-chelating agents such as BAPTA and EGTA, due to depletion of Ca^{2+} and Mn^{2+} from the secretory pathway where they serve essential functions in protein processing, sorting, and glycosylation (10–12). BAPTA toxicity can be overcome by the addition of either Ca^{2+} or Mn^{2+} to the medium, indicating that these two ions play largely surrogate roles in supporting growth (13). However, because Ca^{2+} is present in ~100-fold excess over Mn^{2+} in standard yeast media and because Mn^{2+} is efficiently removed at low chelator concentrations, the observed growth inhibition of *pmr1* mutants by BAPTA represents a titration of available Ca^{2+}. Thus, we have previously demonstrated an excellent correlation between loss of Ca^{2+}

* This work was supported by National Institutes of Health Grant GM62142. The costs of publication of this article were defrayed in part by the payment of page charges. This article must therefore be hereby marked "*advertisement*" in accordance with 18 U.S.C. Section 1734 solely to indicate this fact.

‡ Both authors contributed equally to this work.

§ Current address: Infectious Disease Division, Indian Institute of Chemical Biology, 4 Raja S.C. Mullick Rd., Jadavpur, Calcutta 700032, West Bengal, India.

¶ Current address: HIV Drug Resistance Program, National Cancer Institute-Frederick, P. O. Box B, 1050 Boyle St., Bldg. 535, Rm. 235, Frederick, MD 21702.

‖ To whom correspondence should be addressed: Dept. of Physiology, The Johns Hopkins University School of Medicine, 725 N. Wolfe St., Baltimore, MD 21205. Tel.: 410-955-4732; Fax: 410-955-0461; E-mail: rrao@jhmi.edu.

[1] The abbreviations used are: SPCA, secretory pathway Ca^{2+}-ATPase; SERCA, sarcoendoplasmic reticulum Ca^{2+}-ATPase; PMCA, plasma membrane Ca^{2+}-ATPase; BAPTA, 1,2-bis(2-aminophenoxy)ethane-*N*,*N*,*N*′,*N*′-tetraacetic acid tetrakis; GFP, green fluorescent protein; MES, 4-morpholineethanesulfonic acid.

transport activity in PMR1 mutants and growth sensitivity to BAPTA (14). Loss of Mn^{2+} transport by PMR1 mutants is known to confer hypersensitivity to Mn^{2+} toxicity (14, 15). Although Mn^{2+} is an essential trace element, excess Mn^{2+} is toxic and must be sequestered and removed via the secretory pathway by PMR1 (15). Taken together, growth sensitivities to BAPTA and Mn^{2+} are rapid and effective means to screen *pmr1* mutants for loss of ion transport. Differential sensitivity to BAPTA and Mn^{2+} is potentially indicative of a change in ion selectivity in the mutant, which can then be verified by biochemical characterization.

In a previous study we have described the effects of mutations at Gln-783, positioned at the cytoplasmic interface of transmembrane helix M6 (16). Bulky residues (Leu, Glu, and Thr) could effectively substitute for Gln in the transport of both Ca^{2+} and Mn^{2+} ions. Conversely, introduction of small polar side chains (Ser, Asn, and Cys) at this site led to complete loss of transport, whereas an Ala substitution was unique in conferring a striking and selective loss of Mn^{2+} transport. Evidence for a loss of Mn^{2+} selectivity in the Q783A mutant came from the observed loss of (i) Mn^{2+}-tolerant growth, (ii) Mn^{2+} inhibition of $^{45}Ca^{2+}$ transport, (iii) Mn^{2+}-dependent ATP hydrolysis and phosphoenzyme formation, and (iv) Mn^{2+} inhibition of phosphoenzyme formation from inorganic phosphate. In contrast, BAPTA tolerance, $^{45}Ca^{2+}$ transport, and Ca^{2+}-dependent ATP hydrolysis and phosphoenzyme formation were normal in this mutant (14, 16). *Ab initio* modeling of transmembrane helices M4 and M6 of PMR1 placed Gln-783 (M6) in close proximity to Val-335 (M4) and led us to propose that mutations at position 783 might alter ion selectivity by interfering with helix packing. In this work, we examine additional residues in the vicinity of Gln-783 and specifically test the hypothesis that the interaction between Gln-783 and Val-335 is critical for Mn^{2+} transport.

EXPERIMENTAL PROCEDURES

Media, Strains, and Plasmids—Yeast were grown in minimal medium containing yeast nitrogen base (6.7 g/liter, Difco), glucose (2%), and supplements as needed. Strain K616 (Δ*pmr1*Δ*pmc1*Δ*cnb1* (17)) was used as host; this strain has no endogenous Ca^{2+}-ATPase activity (3). Mutations were introduced in the low copy plasmid YCpHR4 and screened for changes in phenotype (14). This plasmid carries the *PMR1* gene behind a tandem repeat of the yeast heat shock element and directs the expression of low levels of PMR1 in cells cultured at 25 °C. For biochemical assays, the mutations were moved into the multicopy plasmid YEpHisPMR1 from which N-terminal His_9-tagged PMR1 was expressed at moderate levels from the *PGK* promoter (4). This was done by cloning a unique 3.3-kbp *Bam*HI to *Sac*I fragment of the *PMR1* gene containing the desired mutation(s) from YCpHR4 into the same sites on YEpHisPMR1. An N-terminal GFP-tagged version of PMR1 (pSR850) was constructed by cutting pYepHis-PMR1 (the amino-tagged His_9 version of PMR1) with *Mlu*I and *Sac*I and ligated in-frame into plasmid pRA101, which is a 2μ expression plasmid expressing GFP under control of the *PGK* promoter. Mutant proteins were constructed by amplifying the open reading frame of mutant PMR1 from the YCpHR4 vector using a 5′ primer that contained an *Mlu*I site and a 3′ primer that contained a *Sac*I site. The amplified product was purified form was gel-purified, cut with *Mlu*I and *Sac*I, and ligated into *Mlu*I- and *Sac*I-digested pSR850. Sequencing was done to confirm the existence of the intended mutation in the final GFP-tagged construct.

Mutagenesis—In most cases, site-directed mutations in M2, M4, M5, and M6 were generated in either a 1.4-kb *Hin*dIII-*Eco*RI, 1-kb *Bam*HI-*Eco*RI fragment of *PMR1* (M2 or M4) or in a 0.9-kbp *Eco*RI-*Pst*I fragment (M5 or M6) subcloned into pBluescript, sequenced to confirm the mutation, and moved to pYCPHR4 expression plasmid as previously described (*14*). In some cases, the QuikChange site-directed mutagenesis kit (Stratagene) was used to introduce mutations. For random mutations at Val-335, one primer containing random bases at codon 335 was used in conjunction with a complementary primer to generate mutations at this site using the modified cyclical polymerase chain reaction approach of Gama and Breitwieser (18). The fragment was completely sequenced to identify the one or more base substitutions in codon 335 and to rule out unwanted errors that may have been incorporated during *in vitro* synthesis. The fragment was then used to replace the corresponding DNA in YCpHR4. Double mutations at 335 were combined with mutations at residue 783 by subcloning the corresponding fragments into the YCp plasmid. The identity of mutations in the YCp expression plasmid was confirmed to rule out the possibility of unwanted cloning artifacts or wild type sequences.

Phenotype Screens—Growth assays were performed in 96-well plates containing 175 μl of supplemented YNB medium. 2–5 μl of saturated seed culture was incubated at 25 or 30 °C for 2 days. $MnCl_2$ or BAPTA was added to the growth medium at the final concentrations indicated; BAPTA-containing medium was buffered to pH 6.0 with 100 mM MES/HCl. Growth was assessed by measuring absorbance at 600 nm on a Molecular Devices SpectraMax 340 plate reader. Unless otherwise noted, readings were normalized to control samples in which $MnCl_2$ or BAPTA were omitted.

Enzyme Purification and Biochemical Assays—Solubilization and purification of wild type or mutant $(His)_9$-Pmr1 using nickel-nitrilotriacetic acid-agarose (Qiagen) has been described in detail (16). Hydrolysis of [γ-^{32}P]ATP (3000 Ci/mmol, Amersham Biosciences) by purified $(His)_9$-Pmr1 (1 μg) was assayed at 25 °C in buffer containing 50 mM Hepes/Tris, pH 7.0, 100 mM KCl, 1 mM $MgCl_2$, and 50 μM [γ-^{32}P]ATP (500–600 cpm/pmol). $CaCl_2$ or $MnCl_2$ was added and buffered with EGTA to give free cation concentrations that were determined using the WinMaxChelator computer program. Activated charcoal (Sigma) was used to separate free phosphate from ATP, as described earlier (16).

^{54}Manganese Accumulation—Yeast from 2-day-old saturated cultures were inoculated into 500 μl of minimal media with nutrient supplements to yield an initial A_{600} of 0.1 for $n = 3$ wells in a 24-well tissue culture plate. Approximately 1 nM ^{54}MnCl (PerkinElmer Life Sciences, 7600 mCi/mg, ~1.2×10^6 counts/well) was added per well, and yeast were grown at room temperature and assayed for $^{54}Mn^{2+}$ accumulation 24 h post-inoculation by collection onto Millipore 0.45-μm HAWP filters using vacuum filtration. Filters were washed with 10 ml of wash buffer (10 mM HEPES-KOH, pH 7.4, 150 mM KCl), dissolved in 1 ml of dimethylformamide, and counted in 10 ml of scintillation fluid. Yeast growth was measured after 10-fold dilution by absorbance at 600 nm on Genesys 5 spectrometer (Spectronic).

Homology Modeling of PMR1—Homology modeling of *S. cerevisiae* PMR1 (Accession NP_011348) in the E_1 conformation was done using Swiss-PDB viewer (version 3.7b2) by "fitting the raw sequence" of PMR1 to 1EUL.pdb, which is the 2.6-Å resolution crystal structure of *Oryctolagus cuniculus* SERCA1a (accession P04191) in the Ca^{2+}-bound E_1 state (8). Similarly, a homology model of PMR1 in the E_2 conformation was generated using atomic coordinates from 1IWO.pdb for the E_2-like SERCA structure (9). The default alignment settings in Swiss-PDB viewer were used for the initial alignment followed by manual optimization of the alignment to maximize homology between M4 and M5–M7 as shown in Fig. 5. The resulting homology model of PMR1 is based on the Cα positions of 1EUL.pdb and 1IWO.pdb. The single Ca^{2+} ion shown in the model was incorporated by merging the Ca^{2+} ion from site II of the SERCA1a into the aligned regions of PMR1. The images in Fig. 6 were generated by using the rendering program Pov-Ray.

RESULTS

Scanning Mutagenesis of Side Chains Proximal to Gln-783—The unique ion selectivity defect of mutant Q783A prompted a scanning mutagenesis survey of neighboring residues, within a 7-Å radius, based on the E_1 crystal structure of the homologous SERCA1 pump. Specifically, we targeted residues Gln-134, Glu-135, Tyr-136, and Arg-137 of M2, and Phe-738 in M5 that could potentially interact with the Gln side chain at position 783. Each of these residues was replaced with Ala and Ile. Because Gln-783 lies near the cytoplasmic interface of M5, we also performed alanine-scanning mutagenesis of residues in the cytoplasmic half of transmembrane segments M4, M5, and M6. Mutants were expressed from a low copy plasmid in a yeast host strain lacking endogenous Ca^{2+} pumps (K616 (3)) and screened for complementation of BAPTA and Mn^{2+}-hypersensitive phenotypes. Previously, we have assayed ion transport in purified Golgi vesicles and ATP hydrolysis in purified enzyme preparations and demonstrated that these properties correlate with growth sensitivity of mutant strains to BAPTA and Mn^{2+} toxicity (14, 16). Table I depicts $K_{0.5}$ values for BAPTA and

TABLE I
Summary of phenotype screens on PMR1 mutations

Mutations were introduced on a low copy plasmid in a yeast host devoid of endogenous Ca^{2+} pumps. Growth (absorbance at 600 nm) was measured in medium supplemented with a range of BAPTA and Mn^{2+} concentrations as described under "Experimental Procedures." Non-linear curve fitting was done using Origin® (Microcal software) version 6.0 to a one site competition curve: $Y = A_2 + (A_1 - A_2)/1 + 10_0^{x-\log x}$, using normalized growth curve data from one large experiment, which encompassed most of the mutations in this report, with a few exceptions noted below. This minimized lot-to-lot variations in reagents and yeast growth kinetics. Curves were fitted to minimize the least squares value of the calculated curve. The effect of the mutation is summarized in the *box* at the *far right* as follows: *clear*, little or no loss of function; *gray*, moderate loss of function; *black*, severe loss of function. N.D., data not good enough for reliable non-linear curve fitting. Mutant G779T was consistently hypersensitive to BAPTA and Mn^{2+} toxicity, in comparison to wild type.

Membrane Helix	Mutation	$K_{0.5}$ (mM) BAPTA (%)	$K_{0.5}$ (mM) Mn^{2+} (%)	
	WT	1.6 (100)	10.1 (100)	
	Δpmr1	0.3 (19)	2.0 (20)	
M2	Q134A	1.7 (106)	10.2 (102)	
	Q134I	1.3 (81)	7.9 (78)	
	E135A	1.7 (106)	16 (158)	
	E135I	1.6 (100)	10.4 (103)	
	Y136A	1.7 (106)	10.1 (100)	
	Y136I	1.7 (106)	16.4 (162)	
	R137A	0.3 (19)	3.0 (30)	
	R137M	1.2 (75)	5.3 (52)	
M4	L331A	1 (63)	4.2 (52)*2	
	I333A	1.6 (100)	9.7 (96)	
	V335A	1.7 (106)	1.6 (42)*3	
	T336A	1.7 (106)	10.8 (107)	
	V337A	1.7 (106)	11 (109)	
	T338A	1.4 (88)	9.8 (97)	
	L339A	1.2 (75)	5.2 (51)	
	A340K	1.6 (100)	10.2 (101)	
	L341A	0.3 (19)	1.5 (15)	
	G342A	0.9 (57)	N.D.	
	R345A	1.3 (81)	8.3 (82)	
M5	F738A	0.3 (19)	5.2 (51)	
	F738I	0.5 (31)	1.6 (16)	
	F741A	1.2 (75)	5.2 (51)	
	Q742A	0.5 (31)	1.6 (16)	
	L743A	1.3 (81)	10 (99)	
M6	M777A	1.7 (106)	4.6 (46)	
	M777T	1.4 (88)	8.1 (80)	
	G779A	1.5 (94)	4.3 (54)*4	
	G779T	0.1 (6)*1	N.D.	
	P780A	1.8 (113)	7.8 (77)	
	P780L	1.7 (106)	7.8 (77)	
	P781A	1.7 (106)	5.2 (51)	
	L785A	0.7 (44)	2.1 (21)	
	G786A	1.7 (106)	10.2 (101)	
	V787A	1.7 (106)	10.7 (106)	
	E788A	1.2 (75)	7.8 (77)	
	P789A	1.7 (106)	10.9 (108)	
	V790A	1.7 (106)	10.8 (107)	
	D791A	1.8 (113)	10.6 (105)	
	H792A	1.4 (88)	10.6 (105)	

*1 WT BAPTA $K_{0.5}$ of 2.6 mM.
*2 WT Mn^{2+} $K_{0.5}$ of 8.4 mM.
*3 WT Mn^{2+} $K_{0.5}$ of 3.8 mM.
*4 WT Mn^{2+} $K_{0.5}$ of 7.9 mM.

Mn^{2+} for mutants, expressed as percentage of wild type. Substitutions at Gln-134, Glu-135, and Tyr-136 in transmembrane segment M2 had no appreciable effect on PMR1 activity, as judged by their normal or near-normal phenotypes. Only Arg-137 appeared to be sensitive to substitution, and surprisingly, the Ala substitution was more deleterious than the bulkier Met. One mutation in M4, L341A, showed complete loss of

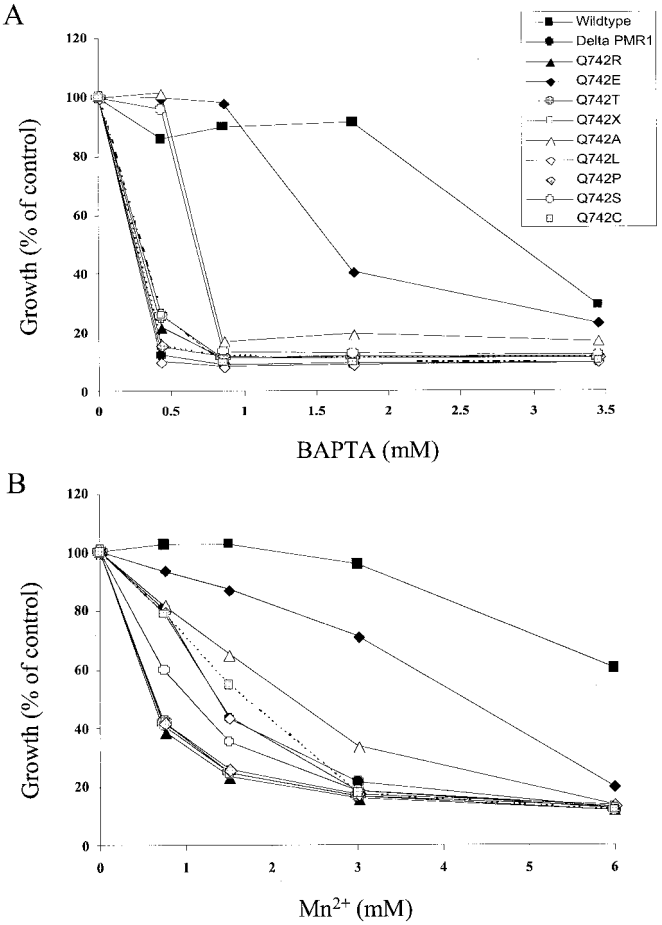

FIG. 1. **Phenotypic effects of substitutions at Gln-742 on BAPTA and Mn^{2+} tolerance.** The host strain K616, carrying null alleles of endogenous Ca^{2+} pumps (Delta PMR1), was transformed with low copy plasmid expressing wild type or mutant PMR1 carrying the indicated amino acid substitutions at position 742. Mutant Q742X has a termination codon at position 742. Cultures were grown in media supplemented with BAPTA (*A*) or Mn^{2+} (*B*). Growth (A_{600}) is expressed as a percentage of control (no BAPTA or Mn^{2+} added).

function when expressed in low copy (Table I) but was similar to wild type when expressed from a multicopy plasmid (not shown). This mutation is therefore likely to have some reduction in turnover that can be compensated by overexpression. Substitution of the evolutionarily conserved Phe-738 at the cytoplasmic interface of M5 by either Ile or Ala led to a complete loss in ability to complement the *pmr1* null phenotypes, from single copy (Table I) or multicopy (not shown) expression plasmids, indicating a critical role for this residue. We had reported earlier that substitution of another residue in M5, Gln-742, with alanine led to a loss of function (14). To investigate the importance of this residue further, we performed random mutagenesis at position 742 and screened the resulting substitutions for BAPTA and Mn^{2+} sensitivity (Fig. 1, *A* and *B*). Of nine different substitutions tested (Arg, Lys, Glu, Thr, Leu, Pro, Ser, Ala, and Cys), only the closely related side-chain Glu could partially replace Gln at this site, whereas all other substitutions led to loss of function.

In M6, mutant L785A, also near the cytoplasmic interface, exhibited a partial loss of function as judged by partial complementation of BAPTA and Mn^{2+} sensitivities in low copy (Table I), and full complementation following high copy expression (not shown). Not surprisingly, mutant G779T located in a conserved motif immediately adjacent to the calcium-binding residue Asp-778 was also inactive. Interestingly, mutant G779A was more sensitive to Mn^{2+} toxicity, relative to BAPTA (Table

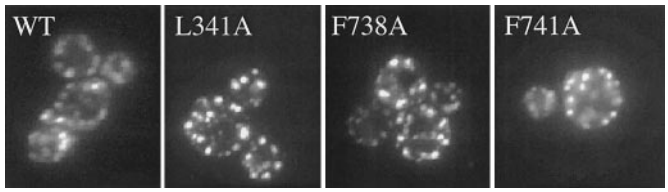

FIG. 2. **Confocal microscopy of yeast expressing GFP-tagged PMR1.** N-terminally tagged PMR1 from wild type and selected mutants were expressed from multicopy plasmids in host strain K616. Live, logarithmically growing cells were examined by confocal microscope as described. The punctate distribution of fluorescence is typical of yeast Golgi bodies. Mutants were essentially similar to wild type.

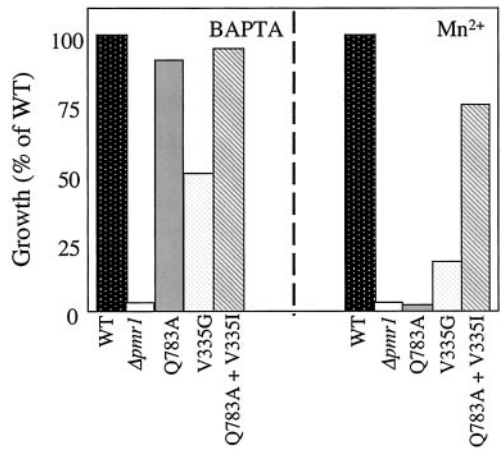

FIG. 3. **Mn^{2+} selectivity mutants.** Growth of the host strain K616 (Δ*pmr1*) transformed with low copy plasmid carrying wild type PMR1 (*WT*) or the indicated single and double mutations was monitored in 1.5 mM BAPTA (*left*) and 3 mM Mn^{2+} (*right*). Growth of the V335I mutant alone was indistinguishable from wild type (not shown). Growth is expressed as percentage of the wild type growth in the same medium. Data are average of duplicate measurements from one representative experiment.

I), suggestive of a change in the relative affinity for Ca^{2+} and Mn^{2+} ions in this mutant. Similarly, analysis of phosphoenzyme formation in the human SPCA1 homologue has revealed that the Hailey Hailey disease mutant G309C in M4 fails to bind Mn^{2+} while retaining reduced Ca^{2+} binding affinity (19). G309C is located immediately proximal to the conserved Glu in the ion binding pocket. It should be noted that most substitutions result in largely similar changes in BAPTA and Mn^{2+} sensitivities (for example, E788A in Table I). This study revealed several potential ion selectivity mutants, including V335A in M4, M777A and P781A in M6, that are worthy of further investigation. Of these, a detailed analysis of Val-335 is reported in this work.

In summary, the scanning mutagenesis identified several hydrophobic residues near the cytoplasmic interface of M4, M5, and M6 that appear to be critical for ion transport. In addition, the requirement for a carboxyl oxygen (from Gln or Glu) suggests that residue Gln-742 may be participate in ion binding. In an earlier study, we had identified several polar or charged residues distributed in the middle tiers of transmembrane helices M4–M8 that might participate in ion binding. The results from this and our previous mutagenesis studies give an increasingly comprehensive picture of the importance of individual residues along the transport pathway.

Subcellular Localization of GFP-tagged PMR1 Mutants—We have previously demonstrated that some loss-of-function PMR1 mutants are retained in the endoplasmic reticulum, where they appear hypersensitive to limited proteolysis by trypsin, indicative of structural or folding defects (14). It was therefore important to determine if mutations reported in this study showed normal biogenesis and trafficking to the Golgi. All mutants showing partial or complete loss of function, were tagged with GFP, and examined by confocal fluorescence microscopy. The mutants showed a punctate distribution typical of yeast Golgi bodies and were essentially identical to wild type (Fig. 2). Thus, loss of function appears to be related to a catalytic, rather than a biogenesis defect.

Substitutions at Val-335 Mimic or Suppress the Mn^{2+} Transport Defect of Mutation Q783A—Based on *ab initio* modeling of M4 and M6 helices, we had suggested earlier that Gln-783 in M6 formed a hydrophobic contact with Val-335 in M4 (16). To test this hypothesis, we generated a series of substitutions at position 335 of PMR1 and analyzed the effect of the mutations by screening for BAPTA and Mn^{2+} toxicity. We found that Cys was not tolerated at 335, whereas residues with large side chains (Thr, Leu, and Ile) were similar to wild type (not shown). These findings were reminiscent of our mutational analysis of residue 783 (16). Interestingly, mutant V335G showed a significant and reproducible difference in response to BAPTA and Mn^{2+} toxicity, indicative of a change in ion selectivity (Fig. 3). A similar trend was observed for the V335A mutation (Table I). Next, we tested whether introduction of the bulkier Ile side chain at residue 335 (V335I) could compensate for loss of side-chain volume in the Q783A mutant. We found that the double mutant V335I/Q783A showed a striking recovery in Mn^{2+}-tolerant growth, relative to that of the single mutant Q783A (Fig. 3). In contrast, mutations in Gln-134, Glu-135, Tyr-136, and Arg-137, also within interacting distance, were ineffective in restoring the Mn^{2+}-sensitive phenotype of mutant Q783A (not shown).

To verify these findings, we measured cation dependence of ATP hydrolysis. Mutants V335G and V335I/Q783A were tagged at the N terminus with a 9xHis epitope and purified by nickel-nitrilotriacetic acid chromatography ("Experimental Procedures"). ATP hydrolysis was assayed as described earlier (16), and the apparent K_m for Ca^{2+} and Mn^{2+} was determined. We have shown earlier that ATPase activity of His-tagged wild type PMR1 is strictly dependent on the presence of calcium (K_m 0.07 μM) or manganese (K_m 0.02 μM) ions (16). Although the apparent affinity for Ca^{2+} was not significantly different from wild type, the V335G mutant showed an 8-fold loss in affinity for Mn^{2+}, consistent with the prediction from the phenotype screen (Table II). Previously, we had shown that Ca^{2+}-dependent ATPase activity in the Q783A mutant was nearly identical to wild type (0.06 μM), whereas Mn^{2+}-ATPase was too low to analyze (16). Table II shows that the apparent K_m for Mn^{2+} in the V335I/Q783A double mutant was similar to wild type, demonstrating an effective correction of the Mn^{2+} transport defect. Thus, engineering a large reduction in side-chain volume at residue 335 (V335G) mimics the Q783A substitution, whereas an increase in side-chain volume (V335I) compensates for the Q783A mutation, consistent with a packing interaction between M4 and M6 at these sites.

Individual Mutations at Residues 335 and 783 in PMR1 Are Incompatible in Combination—To obtain additional evidence for the proposed interaction between residues 335 and 783, we analyzed the effects of various combinations of mutations at these sites by phenotype screening. Table III lists the effects of single and double mutations on growth toxicity of BAPTA (Ca^{2+} transport) and Mn^{2+} (Mn^{2+} transport). Surprisingly, individual mutations that tested similar to wild type were incompatible for BAPTA- and Mn^{2+}-tolerant growth when combined. For example, the single mutants Q783A and V335T displayed normal tolerance to BAPTA, but when combined, the double mutant showed a complete loss of BAPTA tolerance similar to the Δ*pmr1* null strain. The V335T mutation was also inactive in combination with mutations Q783L or Q783E, even

TABLE II
Cation dependence of ATP hydrolysis

His-tagged PMR1 enzymes were purified and the cation dependence of ATP hydrolysis was measured as described under "Experimental Procedures." K_M was derived from a fit of the data to the equation, $v = V_{max} \times S/(K_M + S)$ (16). Mutant V335I was indistinguishable from wild type in the phenotype screens and was therefore not assayed.

PMR1	$Mn^{2+}K_M$	$Ca^{2+}K_M$
	μM	
Wild type	0.02 ± 0.006	0.07 ± 0.001
Q783A	ND[a]	0.06 ± 0.001
V335G	0.16 ± 0.02	0.12 ± 0.05
V335I/Q783A	0.02 ± 0.007	0.09 ± 0.02

[a] ND, not detectable; Mn^{2+}-stimulated ATPase activity was too low to measure (16).

though each of these mutations had normal or near normal phenotype alone. Similarly, the Q783A and V335A double mutant had lower than expected growth in the phenotype screens. In the latter case, we observed an improvement by substituting the Q783L mutation in combination with V335A. Taken together, our results illustrate that combinations of side chains at positions 335 and 783 can either ameliorate or exacerbate the effects of individual substitutions.

Side Chains at Positions 335 and 783 Cannot be Interchanged without Loss of Ion Selectivity and Transport—We reasoned that if the proposed interaction between Gln-783 and Val-335 is conformationally stable, it would be possible to retain function if the side chains were switched. For example, residues forming a non-essential ion pair in the Lac permease could be interchanged without loss of function, although individual substitutions at these sites led to abolishment of transport (20). However, pairs of interacting residues in Lac permease that were predicted to be conformationally mobile could not be interchanged without loss of activity (20). Fig. 4*A* shows the result of phenotype screening of single mutants V335Q, Q783V, and the double mutant. We show that mutation Q783V has near normal growth properties, consistent with our earlier observation that substitutions with other hydrophobic residues (Leu and Ile) were readily tolerated at this position (16). In contrast, mutant V335Q displayed an apparent loss of Mn^{2+} selectivity, as judged by a large reduction in tolerance to Mn^{2+}, but not to BAPTA. We also demonstrate an accumulation of ^{54}Mn in this mutant, similar to that of the Δ*pmr1* null strain, consistent with a loss of Mn^{2+} transport (Fig. 4*B*). Again, we show that a mutation at position 335 is capable of conferring selective loss of Mn^{2+} transport, similar to that seen at position 783. Fig. 4*A* shows that growth sensitivity resulting from the V335Q mutation to BAPTA or Mn^{2+} was not compensated by introduction of the corresponding Q783V mutation, rather, the phenotypic changes were exacerbated in the double mutant.

DISCUSSION

The x-ray crystal structure of the SERCA pump at 2.6-Å resolution in the E_1 conformation shows a cluster of membrane helices (M4, M5, M6, and M8), that enclose two binding sites for Ca^{2+} ions, in excellent accordance with predictions from earlier mutagenesis studies (21). Alignment of the amino acid sequence of PMR1 with SERCA reveals an overall similarity of 48%, which rises to 73% in the regions of M4, M5, and M6 (Fig. 5). Residues contributing to Ca^{2+} *Site II* in SERCA are conserved, whereas the *Site I* residues of SERCA have been replaced by non-conservative amino acids in PMR1 (*green* and *red boxes*, Fig. 5). Consistent with this observation, our earlier mutagenesis survey of all charged and polar residues in transmembrane helices M4–M8 of PMR1 revealed the importance of *Site II* residues in ion binding and transport. Thus, substitutions at Asn-774 and Asp-778 in M6 resulted in complete loss of Ca^{2+} and Mn^{2+} transport function, whereas replacement of Glu-329 in M4 with Ala retained low levels of Ca^{2+} transport activity. A reasonable conclusion from these studies is that a single cation binding site, capable of binding both Ca^{2+} and Mn^{2+}, exists in PMR1.

Interestingly, mutant Q783A at the cytoplasmic interface of

TABLE III
Summary of Mn^{2+} and Ca^{2+} phenotypes of single and double mutations at positions 783 and 335 in PMR1

Mutations were introduced into low copy plasmids and expressed in the Ca^{2+}-ATPase null strain K616. Growth was monitored in liquid medium supplemented with a range of $MnCl_2$ and BAPTA, as described under "Experimental Procedures." The results are coded based on similarity to wild type ○, null mutant ●, or intermediate growth ○ grey circle.

783	335	Mn^{2+}	Ca^{2+}
Q	V	○	○
Q783 Single Mutants			
A	V	●	○
L	V	○	○
V	V	◐	○
E	V	◐	◐
T	V	◐	◐
N	V	●	●
C	V	●	●
S	V	●	●
V335 Single Mutants			
Q	G	◐	○
Q	A	◐	○
Q	Q	●	○
Q	T	○	○
Q	I	○	○
Q	L	○	○
Q	C	●	●
Double Mutants			
A	I	○	○
V	Q	●	◐
A	C	●	●
C	C	●	●
A	T	●	●
A	A	◐	◐
A	L	◐	◐
A	G	◐	◐
L	A	◐	○
L	T	●	◐
E	A	●	◐
E	T	●	●

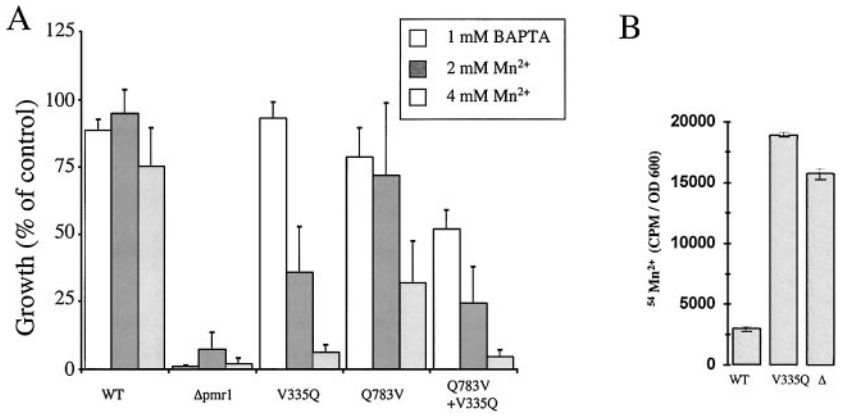

FIG. 4. **Effect of interchanging amino acids at 335 and 783 of PMR1.** *A*, BAPTA and Mn^{2+} tolerance of mutants V335Q, Q783V, and V335Q plus Q783V was examined as described. The data show the mean from $n = 2$ to $n = 4$ separate experiments ± S.E. *B*, ^{54}Mn accumulation was quantitated, as described under "Experimental Procedures," in the yeast null mutant K616 in the absence (Δ), or presence of low copy plasmid expressing wild type PMR1 (*WT*) or the mutant with defective Mn^{2+} tolerance (*V335Q*).

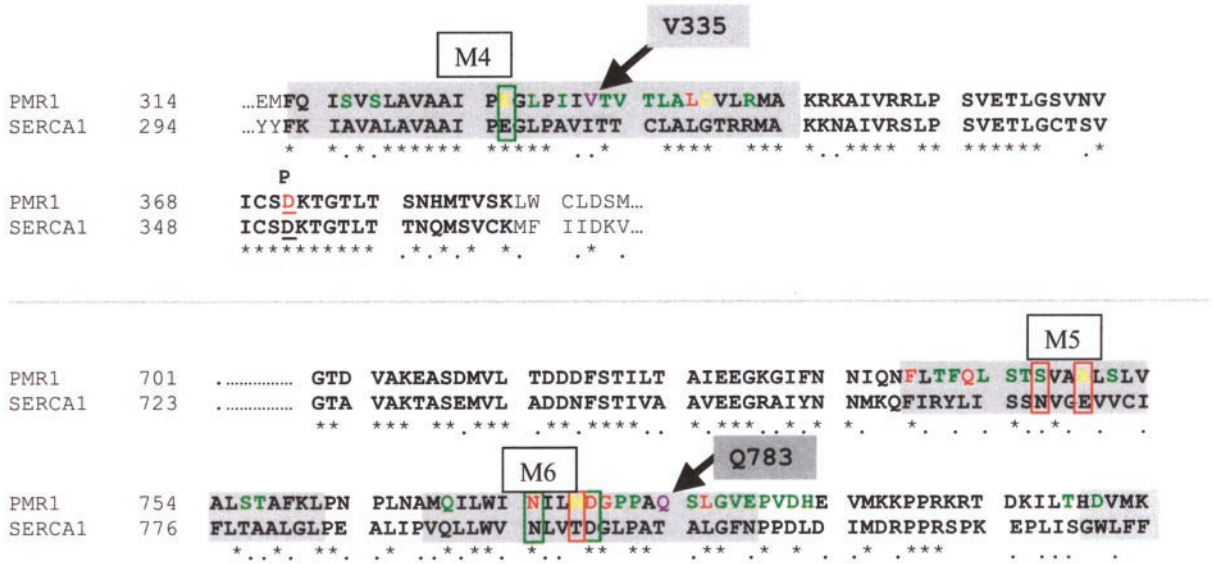

FIG. 5. **Alignment of amino acid sequence of PMR1 and rabbit SERCA1a.** The residues shown in *boldface* were used for homology modeling. Transmembrane helices M4, M5, and M6 are *shaded* in *gray*. Amino acid identity (*) and similarity (.) between the two sequences are indicated. Residues contributing to Ca^{2+} *Site I* and *Site II* in SERCA are *boxed* in *red* and *green*, respectively; note that only *Site II* residues are conserved in PMR1. Residues mutagenized in PMR1 are color-coded *green*, *red*, or *yellow*, based on high, low, or intermediate transport activity (14; this work). Residues Val-335 in M4 and Gln-783 in M6, proposed to interact, are labeled. The phosphorylation site is *underlined* and labeled *P*.

M6, showed nearly complete loss of Mn^{2+} transport, whereas Ca^{2+} transport properties remained normal. Side chain polarity at this position appeared not to be critical, as evidenced by normal phenotypes with both Glu and Leu substitutions. Therefore, it seemed unlikely that Gln-783 directly ligands Mn^{2+} ions, rather, the importance of bulky side chains at this site is indicative of a packing interaction, possibly with M4. Here, we demonstrate that substitutions at residue Val-335, located at the cytoplasmic interface of M4, either ameliorate or exacerbate the effect of substitutions at Q783, consistent with their proximity predicted from a simple *ab initio* model of M4 and M6 (15).

We now take advantage of the recent structural information on the E_1- and E_2-like conformations of SERCA (8, 9) to evaluate the proximity of Val-335 and Gln-783 in homology models of PMR1. Because the validity of homology modeling is dependent on the accuracy of sequence alignment, we have restricted the model to M4, M5, and M6 of PMR1 where sequence similarity with SERCA is very high and continuous (*bold residues*, Fig. 5). The model of the E_1 conformation in Fig. 6*A* shows a single Ca^{2+} ion, occupying *Site II*, with the coordinating residues Asn-774 and Asp-778 (*red*; essential for activity) from M6 and Glu-329 (*yellow*; important for activity) from M4. In the E_2 conformation (Fig. 6*B*), the Ca^{2+} site has been disrupted by the movement of these residues, notably Glu-329, away from the binding pocket. Side chains that may be replaced without significant loss of transport activity are displayed in *green* and can be seen as pointing away from the cation binding site (Fig. 6, *A* and *C*). Substitutions at two residues in M5, Gln-742 and Phe-738, resulted in complete loss of function; strikingly, this model reveals both residues directly extending into the space enclosed by M4, M5, and M6 where they have the potential to influence transport (Fig. 6*C*). The requirement for a Glu or Gln side chain at residue 742 suggests a possible role in ion binding. Gln is conserved at this position in all SPCA and PMCA sequences examined but is replaced by a Leu in the SERCA pumps. Interestingly, PMCA and SPCA are more closely related in having only one ion binding site within the translocation pathway, and it is possible that Gln-742 contributes directly to ion binding or transport in these pumps. The Phe residue at position 738 is conserved in all three classes of calcium pumps and must therefore play a fundamental role in transport. Indeed, our models show a dramatic reorientation of the aromatic ring of Phe-738 from a position perpendicular (in E_1; Fig. 6*C*) to parallel (in E_2; Fig. 6*D*) to the plane of the bilayer. Interestingly, Phe-738 is in the immediate vicinity of Val-335 and Gln-783 in the E_2 structure and may participate in a packing interaction with these residues (see below). The conformation-specific reorientation of the aromatic ring may be important for access of ions from the cytoplasmic side. Taken

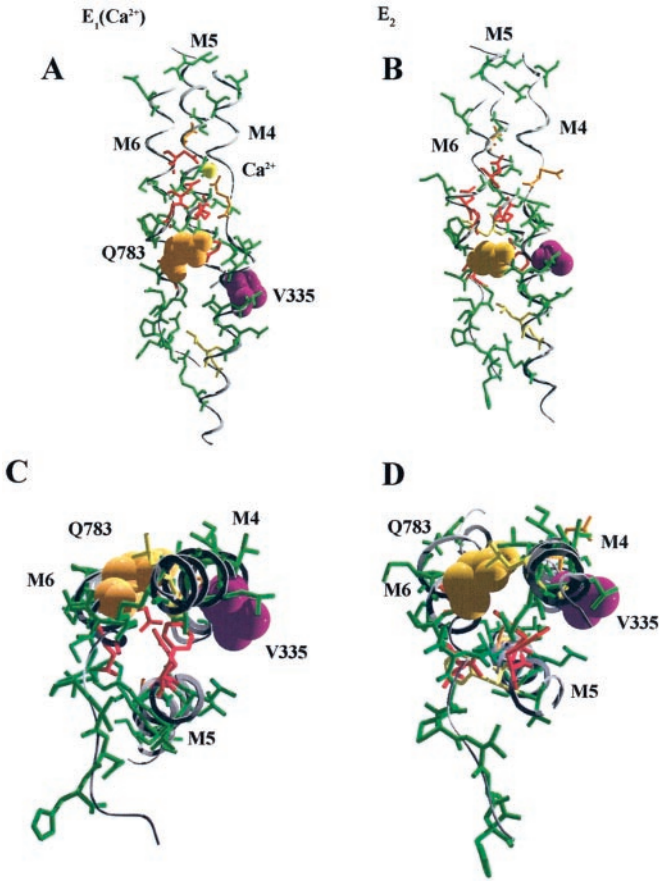

FIG. 6. **E_1 and E_2 conformations of PMR1 showing transmembrane helices M4, M5, and M6.** Homology models of PMR1 were based on the crystal structures of the E_1 and E_2 conformations of SERCA1a and the alignment in Fig. 6 ("Experimental Procedures"). Helices are shown perpendicular to the plane of the membrane (*A* and *B*) or in cross-section from the cytoplasmic side of the membrane (*C* and *D*). Residues Gln-783 (*orange*) and Val-335 (*purple*) are shown in *space-filled* form. A calcium ion (*yellow sphere*) occupying *Site II* in the E_1 conformation has been included. Amino acid side chains are colored *green*, *red*, and *yellow* based on the effect of substitutions reported in this and previous work (Table I and Ref. 14). Residues contributing to the calcium binding site in the E_1 structure are displaced in E_2. Note the movements in the cytoplasmic (*lower*) halves of M4 and M6 that bring Val-335 and Gln-783 in proximity in the E_2 conformation.

together, the placement of the side chains shown in Fig. 6 are remarkably consistent with the results from our mutagenesis studies and support the general validity of homology modeling.

Residues Val-335 and Gln-783 both reside near the cytoplasmic interface, but appear not to interact directly in the E_1 homology model (Fig. 6, *A* and *C*), apparently in contradiction to our experimental findings. Thus, Val-335 is displaced by 120° along the α-helix axis, and one turn away from Gln-783, a distance of nearly 10 Å that is sufficient to preclude a direct interaction between side chains. Similarly, strong cross-links between engineered cysteines in the cytoplasmic half of the membrane spans M4 and M6 of SERCA also cannot be accommodated in the E_1 crystal structure of Toyoshima *et al.* Thus, residue pairs Leu-321 and Gly-808, Thr-317 and Leu-807, and Thr-317 and Ala-804 of SERCA form strong cross-links in the E_2 conformation (22) but are greater than 10 Å apart in the E_1 crystal structure. Importantly, data from these cross-links were used to impose constraints on the *ab initio* modeling of M4 and M6 helices of PMR1 (16), which is therefore likely to be more representative of the E_2 conformation. Remarkably, in the E_2 model (Fig. 6, *B* and *D*), Val-335 and Gln-783 appear in the same tier of helix and are within range of interaction with each other and with Phe-738, as suggested by our mutagenesis data. On the basis of these observations we propose that packing interactions between Val-335, Phe-738, and Gln-783 at the cytoplasmic interface of membrane helices M4, M5, and M6, respectively, influence Mn^{2+} transport.

Given the nature of the amino acid substitutions and the location of these residues close to the membrane interface, it is unlikely that side chains at 783 or 335 directly ligand Mn^{2+} ions. It seems more likely that mutations at these sites can selectively alter access of Mn^{2+} and Ca^{2+} to the binding site. We suggest that the disposition of the side chains of Gln-783 (M6), Val-335 (M4), and F738 (M5) may be critical for both Ca^{2+} and Mn^{2+} access, with individual substitutions having selective effects on these ions. Alternatively, Mn^{2+} and Ca^{2+} may enter the binding pocket through different routes. This would be consistent with our recent demonstration that the SPCA are unique in their ability to mediate high affinity Mn^{2+} transport, whereas retaining similarities to the SERCA and PMCA with respect to Ca^{2+} transport (2). There is evidence suggesting that residues at the cytoplasmic interface of M3 may form a gateway for Ca^{2+} entry in SERCA (23), likewise, Gln-783 and Val-335 may serve a similar role for Mn^{2+} entry in the SPCA. These possibilities may be distinguished by measurements of ion binding and occlusion in future studies. At this time, we note that both Val-335 and Gln-783 are unique and invariant in all known SPCA pumps sequenced to date, underlining their importance to Mn^{2+} transport.

Acknowledgments—We thank Kimberly Young for technical assistance and Van Khue Ton and Thomas Woolf for helpful discussions.

REFERENCES

1. Wuytack, F., Raeymaekers, L., and Missiaen, L. (2003) *Eur. J. Physiol.* **446,** 148–153
2. Ton, V.-K., Mandal, D., Vahadji, C., and Rao, R. (2002) *J. Biol. Chem.* **277,** 6422–6427
3. Sorin, A., Rosas, G., and Rao, R. (1997) *J. Biol. Chem.* **272,** 9895–9901
4. Wei, Y., Marchi, V., Wang, R., and Rao, R. (1999) *Biochemistry* **38,** 14534–14541
5. Hu, Z., Bonifas, J. M., Beech, J., Bench, G., Shigihara, T., Ogawa, H., Ikeda, S., Mauro, T., and Epstein, E. H. (2000) *Nat. Genet.* **24,** 61–65
6. Sudbrak, R., Brown, J., Dobson-Stone, C., Carter, S., Ramser, J., White, J., Healy, E., Dissanayake, M., Larregue, M., Perrussel, M., Lehrach, H., Munro, C. S., Strachan, T., Burge, S., Hovnanian, A., and Monaco, A. P. (2000) *Hum. Mol. Genet.* **9,** 1131–1140
7. East, J. M. (2000) *Mol. Membr. Biol.* **17,** 189–200
8. Toyoshima, C., Nakasako, M., Nomura, H., and Ogawa, H. (2000) *Nature* **405,** 647–655
9. Toyoshima, C., and Nomura, H. (2002) *Nature* **418,** 605–611
10. Rudolph, H. K., Antebi, A., Fink, G. R., Buckley, C. M., Dorman, T. E., LeVitre, J., Davidow, L. S., Mao, J. M., and Moir, D. T. (1989) *Cell* **58,** 133–145
11. Antebi, A., and Fink, G. R. (1992) *Mol. Biol. Cell* **3,** 633–654
12. Dürr, G., Strayle, J., Plemper, R., Elbs, S., Klee, S. K., Catty, P., Wolf, D. H., and Rudolph, H. K. (1998) *Mol. Biol. Cell* **9,** 1149–1162
13. Loukin, S., and Kung, C. (1995) *J. Cell Biol.* **131,** 1025–1037
14. Wei, Y., Chen, J., Rosas, G., Tompkins, D. A., Holt, A., and Rao, R. (2000) *J. Biol. Chem.* **275,** 23927–23932
15. Lapinskas, P. J., Cunningham, K. W., Liu, X., Fink, G. R., and Culotta, V. (1995) *Mol. Cell Biol.* **15,** 1382–1388
16. Mandal, D., Woolf, T., and Rao, R. (2000) *J. Biol. Cell* **273,** 23933–23938
17. Cunningham, K. W., and Fink, G. R. (1994) *J. Cell Biol.* **124,** 351–363
18. Gama L., and Breitwieser, G. E. (1999) *BioTechniques* **5,** 814–816
19. Fairclough, R. J., Dode, L., Vanoevelen, J., Andersen, J. P., Missiaen, L., Raeymaekers, L., Wuytack, F., and Hovnanian, A. (2003) *J. Biol. Chem.* **278,** 24721–24730
20. Sahin-Toth, M., Dunten, R. L., Gonzalez, A., and Kaback, H. R. (1992) *Proc. Natl. Acad. Sci. U. S. A.* **89,** 10547–10551
21. Clarke, D. M., Loo, T. W., Inesi, G., and MacLennan, D. H. (1989) *Nature* **339,** 476–478
22. Rice, W. J., Green, N. M., and MacLennan, D. H. (1997) *J. Biol. Chem.* **272,** 31412–31419
23. Andersen, J. P., Sorensen, T. L., Povlsen, K., and Vilsen, B. (2001) *J. Biol. Chem.* **276,** 23312–23321